Electrocatalytic green ammonia synthesis by nitrate reduction reaction using NiPc–rGO composite

Sourav Paul[1£], Shyamal Murmu[1£], Sourav Bhowmick[1, 2], Supriya Mondal[2*] and Uttam Kumar Ghorai[1*]

[1]Department of Industrial Chemistry & Applied Chemistry, Swami Vivekananda Research Centre, Ramakrishna Mission Vidyamandira, Belur Math, Howrah, 711202, India

[2]Department of Physics, Government General Degree College Chapra, Nadia, West Bengal, 741123, India

*Email: uttam.indchem@vidyamandira.ac.in

*Email: supriyajuphy@gmail.com

£ Equal contribution

Abstract: Converting nitrate, a common water contaminant, into valuable ammonia through electrocatalysis provides a viable substitute for the Haber-Bosch process, with diverse applications and environmental benefits. Although, there are different nitrate reduction routes present, the challenge exists due to the insufficiency of efficient electrocatalysts in controlling the reaction route towards sustainable ammonia synthesis. Herein, we present an active and selective route for reducing nitrate to ammonia on a NiPc_rGO composite catalyst, having a 52% Faradaic efficiency and a rate of ammonia output of 11064 μg h^{-1} mg_{cat}^{-1} at a potential of –0.9 V vs. RHE.

Keywords: *Electrocatalysis; Nitrate reduction; Green Ammonia; Nickel Phthalocyanine.*

1. Introduction:

One of the chemicals with the largest global fabrication output is ammonia, and its market size and value make up 5% of the total value of the chemical industry worldwide. The majority of the ammonia produced is utilized to make chemical fertilizers for use in agriculture. Ammonia serves as a primary component in the production of textiles, pharmaceuticals, explosives, and refrigeration. Ammonia is essential for human life, survival, and growth.[1–3] The Haber-Bosch ammonia synthesis process that is presently used is energy-intensive, and produce a large amount of greenhouse emissions. So, electrochemical nitrogen reduction reaction (NRR) is seen as a very competitive alternative.[4,5] However, the inert character of the N≡N bond, the extremely poor solubility of N_2 molecule in aqueous medium, and the competing hydrogen evolution process (HER) frequently result in restricted FE and a very poor ammonia production rate, rendering inferior electrocatalytic performance.[6–10] From an energy and environmental viewpoint, a sustainable N-containing alternative, nitrate ions (NO_3^-) can be a better alternative than N_2. Due to the following reasons, (a) nitrates are highly soluble in water, (b) have lower bond dissociation energy of 204.0 kJ mol^{-1}, (c) low reaction barrier, electrocatalytic nitrate reduction can occur at the solid–liquid interface. Furthermore, the fact that the nitrogen element in NO_3^- has the greatest oxidation state supports the possibility of a reduction reaction leading to the selective synthesis of NH_4^+. NRR may result in simultaneous intermediate-valence N_2 oxidation and reduction, which reduces the selectivity for NH_4^+.[11–13] Therefore, the process of converting nitrate to ammonia seems to be more facile than NRR. Furthermore, using NO_3^- as a feedstock has the additional benefit of its abundant dispersion in wastewater. Wastewater frequently contains nitrate, which is an adequate reactant for NO_3^- reduction reaction (NO_3RR) pathways.[13–15] Rather than partially reducing NO_3^- to N_2 for purification, the 8-electron exchange process for NO_3RR ($NO_3^- + 9H^+ + 8e^- \rightarrow NH_3 + 3H_2O$) gives the opportunity for the conversion of contaminated NO_3^- into a value-added product. Therefore, the NO_3RR route for ammonia production, offers sustainable nitrogen-cycle employment, has a notable impact on lowering energy consumption

while easing environmental concerns. High FE towards ammonia is strongly sought because the reaction has numerous intermediates and progresses through the transfer of 9 protons and 8 electrons.[16] Although the NO_3RR route is a popular but challenging area of current research, it has several unavoidable drawbacks. Strong competitive side reactions, primarily connected to the 5-electron handover for the partial reduction of NO_3^- ions to N_2 and the hydrogen evolution reaction (HER), may accompany the 8-electron addition reaction for the formation of NH_4^+ from NO_3^- .[17,18] Furthermore, it is widely acknowledged that the main factors affecting the rate of yield and selectivity of ammonia are the development of new catalytic materials, accurate control of the reaction's variables, and thorough study of the reaction's mechanism. For a comprehensive catalysis system to successfully support catalytic performance, a logical design is therefore required.

In response to these challenges, scientists have invented various catalysts, like defect site engineering in heterostructure interface (CuPc-CeO_2),[19] 2D iron-cyano catalyst with hydrophilic surface,[18] transition metal (TM) complexes where TM centre functions as the primary site for electrochemical reduction reactions, while the organic cyclic ring prevents the occurrence of competing hydrogen evolution reactions (HER).[3,5] Therefore drawing inspiration from the various strategies we investigated on the aspect of inhibiting HER by introducing a non-metallic constituent, and promoting NO_3RR via the TM centre. Herein, we showed a general strategy to synergistically combine the unique properties of two–dimensional materials (rGO) and transition metal phthalocyanine; to capitalize on the strong interfacial interplay between the rGO surface and NiPc, which leads to facile charge transfer, efficient proton coupled electron transfer which is vital for reduction processes.[20–24] As far as we know, the NiPc_rGO catalyst has not been investigated as an effective electrocatalyst for electrochemical NO_3RR to ammonia before. The NiPc_rGO catalytic system displayed remarkable electrochemical durability and structural stability, and it obtained an excellent ammonia yield rate of 11064 $\mu g\ h^{-1}\ mg_{cat}^{-1}$ and FE of 52% at a potential of –0.9 V (vs. RHE).

2. Experimental details:

2.1 Materials

Phthalonitrile (Sigma Aldrich), nickel (II) acetate (Merck), ethylene glycol (Merck), ammonium heptamolybdate tetrahydrate (Merck), hydrazine hydrate (Sigma Aldrich), sodium hypochlorite solution (Merck), sodium nitroprusside dihydrate (Loba Chemie) sodium hydroxide (Merck), salicylic acid (Merck) and trisodium citrate were used without any additional purification.

2.2 Catalyst synthesis

A recent demonstration has highlighted the facile synthesis of nickel phthalocyanine via a solvothermal route. This method utilizes metal salts like nickel acetate and an organic precursor, phthalonitrile, in an ethylene glycol solvent medium, enabling the preparation of transition metal-based electrocatalysts.[5] Graphene oxide (GO) was prepared via a modified Hummers' method. The obtained GO dispersed in DMF, was treated with a solution of hydrazine hydrate in ammoniacal solution at 90 °C to reduce it to reduced graphene oxide (rGO).[24] NiPc and rGO were mixed in equal parts and suspended in isopropyl alcohol. The NiPc–rGO catalyst was created by centrifuging the material that was left over after the solution was mixed for a few hours and repeatedly washing it with deionized water.[24]

2.3 Instrumentation

Using a Bruker D-8 advanced Eco X-ray powder diffractometer (voltage 40 kV, current 25 mA, λ=0.15404 nm radiation of Cu-K_α), the phase purity of the synthesised NiPc–rGO catalyst was examined using XRD characterisation technique. The IRAffinity-1S FTIR spectrometer (Shimadzu) was used to examine the chemical bonds in the synthesised NiPc–rGO system. The Shimadzu UV-3600 Plus spectrophotometer was used to analyse the absorbance spectroscopy data.

2.4 Electrochemical nitrate reduction

An electrochemical workstation (Model No. CHI760E) along with a three-electrode arrangement in an H-type cell divided by a proton-exchangeable

Nafion 117 membrane was used to analyse the electrochemical experiments in ambient circumstances. Pt foil and Ag/AgCl (3.5 M saturated KCl) were taken as the counter and reference electrodes, respectively. All electrochemical tests were executed at standard temperature and pressure. For the nitrate reduction reaction, 0.1 M $NaNO_3$ and 0.1 M Na_2SO_4 was considered as electrolytes.

The following relation was used to shift all applied potentials from Ag/AgCl to the standard hydrogen electrode: E (vs. RHE) = E (vs. Ag/AgCl) + (0.059 V × pH) + 0.198 V.

2.5 Product Analysis

Quantification of ammonia: The indophenol blue spectrochemical method was applied to quantitatively measure the ammonia concentration using UV-visible spectroscopy. First, 2 ml of the 100 times diluted electrolyte collected after chronoamperometry was mixed with 1 ml of the oxidizer solution made with a 0.05 M sodium hypochlorite solution. Next, 0.2 ml of catalyst was added using a 3.34 mM sodium nitroprusside dihydrate solution. Next, 2 ml of a colourant solution was added. This solution was created by adding 1 M sodium hydroxide solution to 5 weight percent salicylic acid solution and 5 weight percent trisodium citrate. After two hours of incubation at room temperature, the solution's absorbance was assessed. The maximum absorbance in the UV-vis data was observed at 655 nm, suggesting that indophenol blue had formed. A calibration series was created by plotting an ammonium sulphate solution with different concentrations ranging from 1.0, 0.8, 0.6, 0.4, 0.2, and 0.0 (µg/ml)} in 0.1 M Na_2SO_4 and 0.1 M $NaNO_3$ solution. The plot of absorbance vs. concentration was then created using UV–vis data **(Figure 1a)**. The absorbance and concentration have a linear relationship (y = 0.2442x + 0.03987; R^2 = 0.997) in **Figure 1b**.

Quantitative estimation of hydrazine: For hydrazine quantitation, the Watt and Chrisp method was used.[25] Typically, 300 ml of absolute ethanol, 5.99 g of para (dimethylamino) benzaldehyde, and 30 ml of concentrated HCl were combined to create a coloured solution. 4 ml of the coloured solution and 1 ml of the analyte solution were then added. After incubating for around 15 minutes, the mixture's UV-vis absorbance spectrum data were acquired, with the highest absorption at 455 nm. The following steps were used in the preparation of the calibration solution series: Initially, hydrazine-monohydrate standard solutions were made with concentrations ranging from 0.0, 0.2, 0.4, 0.6, 0.8, and 1.0 (µg/mL) (**Figure 1c**). Then, after addition of the prepared coloured solution to the calibrated hydrazine monohydrate solution(s) it was nurtured in the dark for around 15 minutes at RT. The maximum absorbance in the UV-vis spectral data was observed at 455 nm. When absorbance and hydrazine-monohydrate concentrations were plotted against one another, a straight line (y = 0.20614x + 0.0087; R^2 = 0.996) was produced (**Figure 1d**).

Equation for the rate of ammonia yield and Faradaic efficiency determination

It is necessary to quantify the ammonia generated during electrocatalysis; the following equations were utilised to perform the calculation:

$$R_{NH_3} = \frac{(C_{NH_3} \times V)}{(m_{cat} \times t)} \quad \ldots\ldots\ldots\ldots\ldots\ldots\ldots (1)$$

Where C_{NH_3} is the ammonia concentration. The electrolyte volume is denoted by V, the catalyst mass placed on carbon paper is represented by m_{cat}, and the reaction duration is denoted by t.

$$FE (\%) = \frac{(8 \times V \times C_{NH_3} \times F)}{(17 \times Q)} \times 100\% \ldots\ldots\ldots\ldots\ldots\ldots (2)$$

Here, F stands for Faraday constant, C_{NH_3} is the ammonia concentration, V refers to the electrolyte volume used for each reaction, and Q refers to the total charge on the electrode surface.

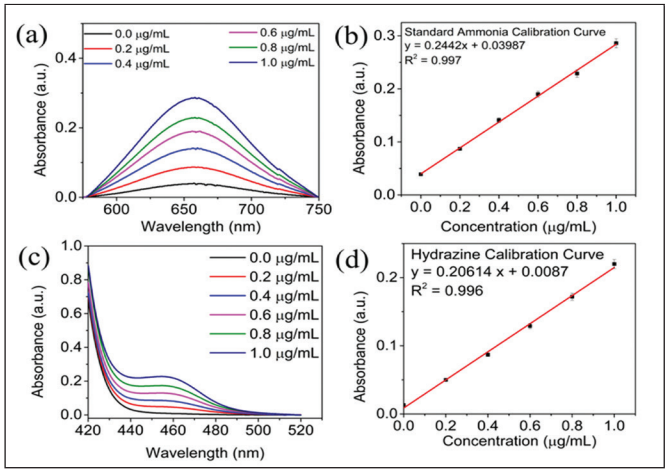


Figure 1. Ammonia's UV-vis calibration curve utilising standards of ammonium sulphate solutions at known concentrations: (a) the indophenol assays' UV-vis curves containing NH_4^+ ions after two hours of incubation and (b) calibration curve used for ammonia estimation by NH_4^+ ions of different concentrations. UV-vis calibration curve of N_2H_4 of known concentration as standards (c) UV-vis absorption spectra at different concentrations of standard hydrazine during a 15-minute incubation period in ambient circumstances (d) The standard calibration curve for hydrazine content determination.

3. Results and Discussion

3.1 Characterization of catalyst: The produced NiPc_rGO electrocatalyst was investigated by XRD, and **Figure 2** illustrates the XRD spectrum of NiPc system, and also the rGO component.

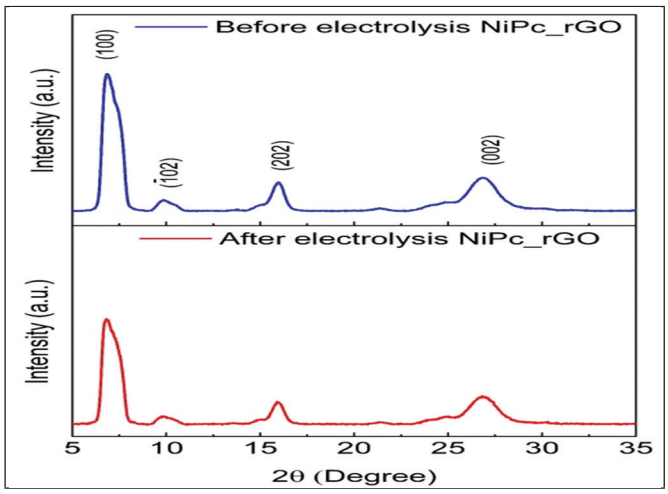


Figure 2. XRD pattern of NiPc–rGO catalytic system

Figure 2 corresponds to the NiPc and rGO in accordance to their reported diffraction peaks, with major reflections around 6.7°, 9.6° and 15.8° corresponding to the reflections from the (100), ($\bar{1}$02) and (202) planes of NiPc respectively, and the broad diffraction peak at ~26° indicates the presence of (002) plane of reduced graphene oxide.[24] Furthermore, to assess the stability of the catalyst, the XRD study was carried out after electrochemical NO_3RR process; **Figure 2** also reveals the XRD pattern after NO_3RR process, which showed no such significant change in the diffraction peaks which demonstrates structural durability of NiPc_rGO catalyst. "The bending of in-plane benzene is represented by the peak at 1118 cm-1 in the FTIR spectra (Figure 3), whereas the Ni–N bond seen in NiPc is associated with the peak at 1165 cm-1." The C-N-C bridges are associated with the primary peak at 1335 cm^{-1}, whereas the stretching of C-C bonds in pyrrole are correlated with the peak at 1428 cm^{-1}.[5] The positive interaction between the π–π stacking interactions and the NiPc's non-covalent interaction with the rGO reduces the strength of the peaks.

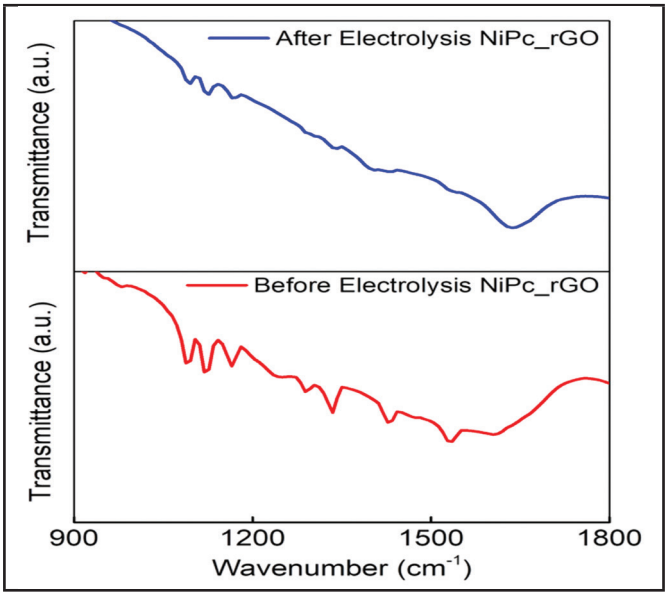


Figure 3. FTIR spectra of NiPc–rGO catalytic system

3.2 Performance of the electrochemical nitrate reduction process

In an H-cell, electrocatalytic nitrate reduction was performed. NiPc–rGO (0.2 mg catalyst) was

coated over carbon paper (1× 1 cm^2) to serve as the working electrode. First, we employed linear sweep voltammetry in Na_2SO_4 electrolyte with and without $NaNO_3$ to examine the nitrate reduction activity of NiPc–rGO (**Figure 4a**). The obvious rise in current density at the same potential suggests that nitrate ion reduction by the NiPc–rGO may be effective. In order to assess the product selectivity, chronoamperometry (CA) studies were performed in 0.1 M Na_2SO_4/0.1 M $NaNO_3$ electrolyte at specified potentials each time for an hour, with generated NH_3 products quantified by spectrophotometry.

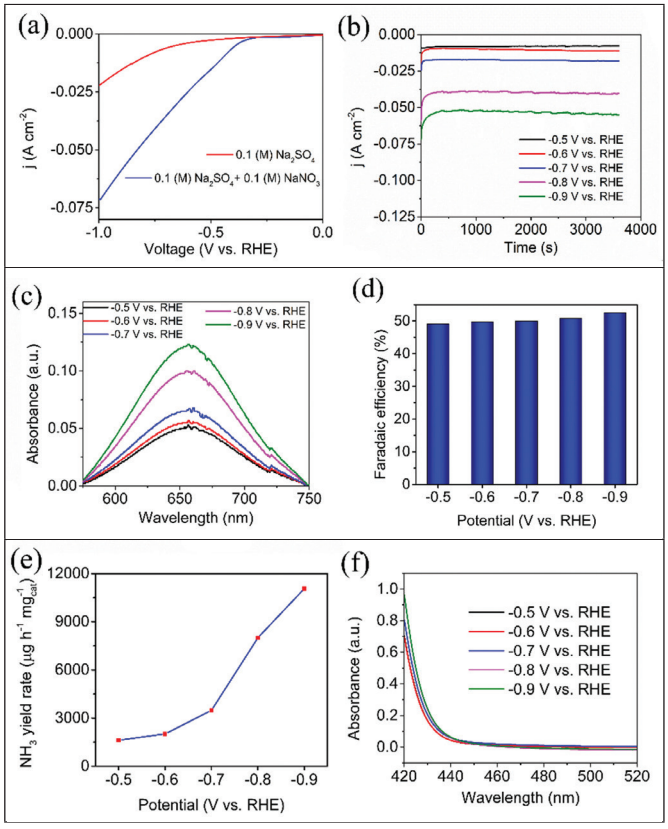


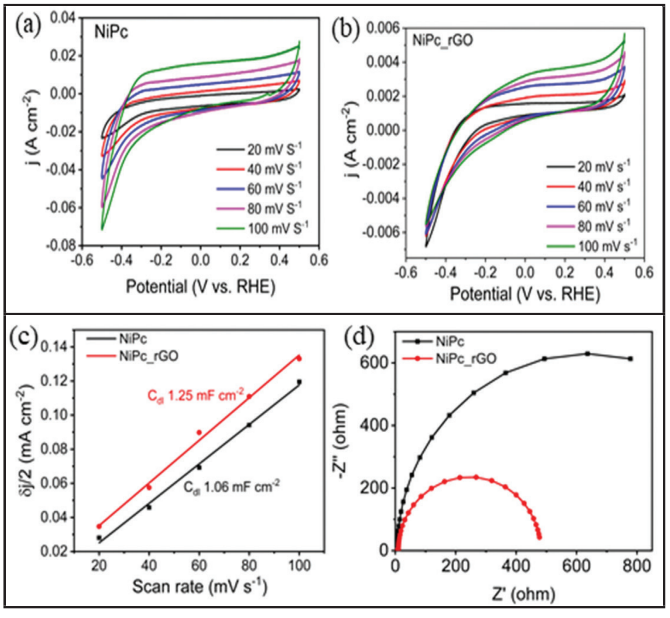
Figure 4. Electrochemical nitrate reduction activity. (a) LSV curves of the NiPc_rGO in 0.1 M Na_2SO_4 electrolyte and 0.1 M Na_2SO_4/0.1 M $NaNO_3$ mixed electrolyte. (b) Current density and reaction time at different potentials of NiPc–rGO (c) UV-visible absorption spectra of the electrolytes at different potentials after 3600 sec NO_3RR electrolysis. (d) NH_3 FE of NiPc_rGO at each given potential. (e) NH_3 yield rate at various potentials using NiPc–rGO catalyst. (f) UV–vis spectra of electrolytes for detecting N_2H_4.

The CA study (**Figure 4b**) showed insignificant fluctuations of current density with respect to time implying that stable current is maintained by the catalyst which aids in the process of efficient nitrate reduction reaction, via constant supply of electrons to the nitrate ions uniformly which facilitates the process of nitrate reduction. **Figure 4c** illustrates the UV-visible spectra with a maximum absorption at 655 nm verifying the electrochemical nitrate reduction at various potentials ranging from –0.5 V to –0.9 V. The rate of NH_3 generation and FE of generated NH_3 were quantitatively measured using the indophenol blue technique. As seen in **Figure 4c**, our NiPc–rGO catalyst exhibits great selectivity and a better yield rate for electrocatalytic NO_3^- to NH_3 conversion. The NH_3 product can be easily identified in **Figure 4d,** with a FE of 50%, corresponding to a yield rate of 3478 μg h^{-1} mg_{cat}^{-1} (**Figure 4e**) at the reaction carried out at –0.70 V vs. RHE with an average current density of 0.018 A cm^{-2}). The yield rate is 11064 μg h^{-1} mg_{cat}^{-1} as the NH_3 selectivity steadily rises to a 52% at –0.9 V with an average current density of 0.055 A cm^{-2}. **Figure 4f** verifies the excellent selectivity of the catalyst for converting NO_3^- to NH_3, revealing that no such absorbance is present at 455 nm in the UV-vis spectrum, indicating that hydrazine (N_2H_4) is not formed during the NO_3RR process. It also shows that ammonia formation is preferred over hydrazine formation with negligible amounts of the latter occurring. Due to the radically different kinetical energy barriers to overcome,[26] the rate of yield and FE of NO_3^- to NH_3 conversion on NiPc_rGO are orders of magnitude larger than the reported N_2 to NH_3 conversions.

3.3 Control Experiment

The NiPc–rGO and NiPc catalyst system's cyclic voltammetry (CV) curves, shown in Figures 5a and 5b, respectively, were examined to find the current density at different sweep speeds (20, 40, 60, 80, and 100 mV s^{-1}) within the potential range of –0.5V to 0.5V vs. RHE. The electrochemical double layer capacitance (C_{dl}) was then computed using the data that was taken out of the CV plots. To find the electrochemical surface area (ECSA) of NiPc–rGO and NiPc, the C_{dl} was measured.[27,28] The

C_{dl} value for NiPc–rGO (1.25 mF cm^{-2}) significantly exceeds that of the NiPc (1.06 mF cm^{-2}), as **Figure 5c** illustrates. This result suggests that NiPc–rGO exhibits a greater number of active sites compared to pristine NiPc, thereby indicating its enhanced NO_3RR activity relative to NiPc. Additionally, the charge transfer resistance (R_{ct}) during NO_3RR operation was investigated using electrochemical impedance spectroscopy (EIS). **Figure 5d** presents the EIS findings for the NiPc–rGO system, indicating a much smaller semicircle compared to NiPc. This suggests that NiPc–rGO, exhibits lower charge transfer resistance and reduced electron transfer impedance.[29,30] Additionally, we assessed the ammonia yield through the NO_3RR process at the potential of -0.9 V vs. RHE using three distinct control systems aside from NiPc–rGO. As depicted in **Figure 5e,** the maximum NH_3 yield of 11064 μg h^{-1} mg_{cat}^{-1} was observed for NiPc–rGO, while for other control systems such as NiPc, rGO, and carbon paper, the NH_3 yield was measured at 6374, 1985, and 212 μg h^{-1} mg_{cat}^{-1}, respectively. To assess the durability of the electrocatalyst, a prolonged chronoamperometry test was performed at −0.9 V for 5 hours for 5 cycles. As depicted in **Figure 5f,** minimal fluctuation in current density was observed, pointing that the composite catalyst exhibited stable electrocatalytic activity without significant variations in the current density throughout the electrochemical reaction.



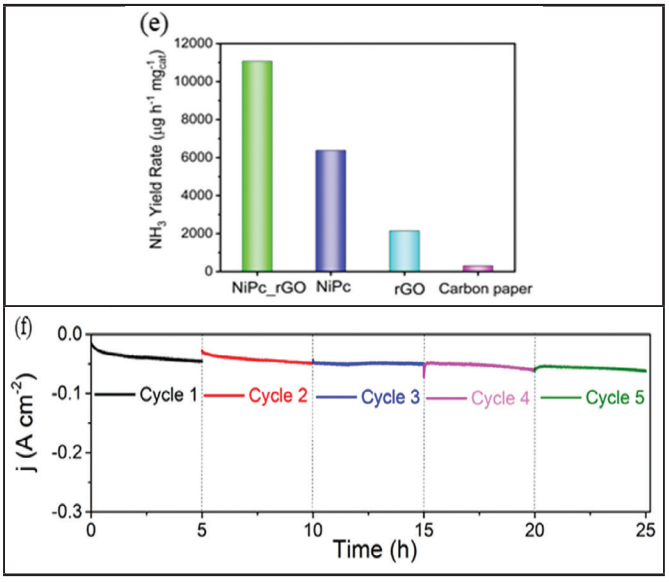


Figure 5. Control experiment. (a) Cyclic voltametric plot of NiPc, (b) Cyclic voltametric plot of NiPc–rGO at varying sweep rates, (c) Plot of the variance in current density (δj/2) against scan rate for determining the C_{dl} values, (d) EIS spectra for NiPc, and NiPc–rGO, (e) The bar diagram illustrates the control experiments at –0.9V vs RHE for rGO, carbon paper, NiPc, and NiPc–rGO, (f) 5 time recycling electrochemical tests for 5 h long term chronoamperometry curves of NiPc–rGO.

4. Conclusions: Nitrate pollution could be reduced using electrochemical nitrate reduction to ammonia synthesis under ambient conditions. Effective catalysts are needed because of the nitrate-to-ammonia reaction's slow kinetics. Our synthesized composite NiPc_rGO catalyst demonstrated a high degree of selectivity and stability, resulting in an ammonia yield rate of 11064 μg h^{-1} mg_{cat}^{-1} and a FE of 52% at –0.9 V vs. RHE. This work provides a fresh approach to the tactical planning of an electrocatalytic nitrate reduction to ammonia system based on transition metal phthalocyanine supported by conducting carbon support in an ambient environment.

Acknowledgements:

SM acknowledges SERB, Govt. of India, for providing the financial support (EEQ/2022/001082). SM wishes to thank Dr. Subhasis Panda, Principal, Government General Degree College Chapra, for his endless and enthusiastic support towards this project.

References:

[1] A. Good, Toward nitrogen-fixing plants, Science, 359 (2018), 869-870. https://www.science.org/doi/10.1126/science.aas8737.

[2] J. Lim, C.A. Fernandez, S.W. Lee, M.C. Hatzell, Ammonia and Nitric Acid Demands for Fertilizer Use in 2050, ACS Energy Lett., 6 (2021), 3676−3685. https://doi.org/10.1021/acsenergylett.1c01614.

[3] U.K. Ghorai, S. Paul, B. Ghorai, A. Adalder, S. Kapse, R. Thapa, A. Nagendra, A. Gain, Scalable Production of Cobalt Phthalocyanine Nanotubes: Efficient and Robust Hollow Electrocatalyst for Ammonia Synthesis at Room Temperature, ACS Nano, 15 (2021), 5230-5239. https://doi.org/10.1021/acsnano.0c10596.

[4] C. Tang, S.Z. Qiao, How to explore ambient electrocatalytic nitrogen reduction reliably and insightfully, Chem. Soc. Rev., 48 (2019), 3166−3180. https://doi.org/10.1039/C9CS00280D.

[5] S. Murmu, S. Paul, S. Kapse, R. Thapa, S. Chattopadhyay, A. Nagendra, S.N. Jha, D. Bhattacharyya, U.K. Ghorai, Unveiling the genesis of the high catalytic activity in nickel phthalocyanine for electrochemical ammonia synthesis J. Mater. Chem. A, 9 (2021), 14477-14484. https://doi.org/10.1039/D1TA00766A.

[6] N. Zhang, L. Li, J. Wang, Z. Hu, Q. Shao, X. Xiao, X. Huang, Surface-Regulated Rhodium–Antimony Nanorods for Nitrogen Fixation, Angew. Chem., Int. Ed., 59 (2020), 8066. https://doi.org/10.1002/anie.201915747.

[7] S. Paul, S. Sarkar, A. Adalder, A. Banerjee, U. K. Ghorai, Dual metal site-mediated efficient C–N coupling toward electrochemical urea synthesis, J. Mater. Chem. A, 11 (2023), 13249-13254. https://doi.org/10.1039/D3TA01011B.

[8] Z. Geng, Y. Liu, X. Kong, P. Li, K. Li, Z. Liu, J. Du, M. Shu, R. Si, J. Zeng, Achieving a Record-High Yield Rate of 120.9 μg_{NH3} mg_{cat}^{-1} h^{-1} NH_3 for N_2 Electrochemical Reduction over Ru Single-Atom Catalysts, Adv. Mater., 30 (2018), 1803498. https://doi.org/10.1002/adma.201803498.

[9] Y. J. Jang, A. E. Lindberg, M. A. Lumley, K.-S. Choi, Photoelectrochemical Nitrogen Reduction to Ammonia on Cupric and Cuprous Oxide Photocathodes, ACS Energy Lett., 5 (2020), 1834–1839. https://doi.org/10.1021/acsenergylett.0c00711.

[10] J. Mukherjee, A. Adalder, N. Mukherjee, U. K. Ghorai, Solvothermal synthesis of α–CuPc nanostructures for electrochemical nitrogen fixation under ambient conditions, Catal. Today, 423 (2023), 113905. https://doi.org/10.1016/j.cattod.2022.09.011.

[11] L. Li, C. Tang, X. Cui, Y. Zheng, X. Wang, H. Xu, S. Zhang, T. Shao, K. Davey, S.Z. Qiao, Efficient Nitrogen Fixation to Ammonia through Integration of Plasma Oxidation with Electrocatalytic Reduction, Angew. Chem. Int. Ed., 60 (2021), 14131–14137. https://doi.org/10.1002/anie.202104394.

[12] H. Hirakawa, M. Hashimoto, Y. Shiraishi, T. Hirai, Selective Nitrate-to-Ammonia Transformation on Surface Defects of Titanium Dioxide Photocatalysts, ACS Catal., 7 (2017), 3713–3720. https://doi.org/10.1021/acscatal.7b00611.

[13] S. Paul, S. Sarkar, A. Adalder, S. Kapse, R. Thapa, U. K. Ghorai, Strengthening the Metal Center of Co–N_4 Active Sites in a 1D–2D Heterostructure for Nitrate and Nitrogen Reduction Reaction to Ammonia, ACS Sustainable Chem. Eng., 11 (2023), 6191-6200. https://doi.org/10.1021/acssuschemeng.2c07114.

[14] L. Zhou, Y. Jiang, Y. Wan, X. Liu, H. Zhou, W. Li, N. Li, Xin Wang, Electron Flow Shifts from Anode Respiration to Nitrate Reduction During Electroactive Biofilm Thickening, Environ. Sci. Technol., 54 (2020), 9593–9600. https://doi.org/10.1021/acs.est.0c01343.

[15] N. C. Kani, J. A. Gauthier, A. Prajapati, J. Edgington, I. Bordawekar, W. Shields, M. Shields, L. C. Seitz, A. R. Singh, M.R. Singh, Solar-driven electrochemical synthesis of ammonia using nitrate with 11% solar-to-fuel efficiency at ambient conditions, Energy Environ. Sci., 14 (2021), 6349–6359. https://doi.org/10.1039/D1EE01879E.

[16] J.-X. Liu, D. Richards, N. Singh, B. R. Goldsmith, Activity and Selectivity Trends in Electrocatalytic Nitrate Reduction on Transition Metals, ACS Catal., 9 (2019), 7052. https://doi.org/10.1021/acscatal.9b02179.

[17] Y. Wang, W. Zhou, R. Jia, Y. Yu, B. Zhang, Unveiling the Activity Origin of a Copper-based Electrocatalyst for Selective Nitrate Reduction to Ammonia, Angew. Chem. Int. Ed., 59 (2020), 5350–5354. https://doi.org/10.1002/anie.201915992.

[18] P. Li, Z. Jin, Z., Fang, G. Yu, A single-site iron catalyst with preoccupied active centers that achieves selective ammonia electrosynthesis from nitrate, Energy Environ. Sci., 14 (2021), 3522–3531. https://doi.org/10.1039/D1EE00545F.

[19] X. Li, W. Fan, Y. Bai, Y. Liu, F. Wang, H. Bai, W. Shi, Photoelectrochemical reduction of nitrate to ammonia over CuPc/CeO_2 heterostructure: Understanding the synergistic effect between oxygen vacancies and Ce sites, Chem. Eng. J., 433 (2022), 133225. https://doi.org/10.1016/j.cej.2021.133225.

[20] W. Liao, L. Qi, Y. Wang, J. Qin, G. Liu, S. Liang, H. He, L. Jiang, Interfacial Engineering Promoting Electrosynthesis of Ammonia over Mo/Phosphotungstic Acid with High Performance, Adv. Funct. Mater., 31(2021), 2009151. https://doi.org/10.1002/adfm.202009151.

[21] Q. Li, Y. Zhang, X. Wang, Y. Yang, Dual Interface-Engineered Tin Heterostructure for Enhanced Ambient Ammonia Electrosynthesis, ACS Appl. Mater. Interfaces, 13 (2021), 15270–15278. https://doi.org/10.1021/acsami.1c01160.

[22] J. Yin, Z. Gao, F. Wei, C. Liu, J. Gong, J. Li, W. Li, L. Xiao, G. Wang, J. Lu, L. Zhuang, Customizable CO_2 Electroreduction to C_1 or C_{2+} Products through Cu_y/CeO_2 Interface Engineering, ACS Catal., 12 (2022), 1004–1011. https://doi.org/10.1021/acscatal.1c04714.

[23] H. Ma, Z. Chen, Z. Wang, C. V. Singh, Q. Jiang, Interface Engineering of Co/CoMoN/NF Heterostructures for High-Performance Electrochemical Overall Water Splitting, Adv. Sci., 9 (2022), 2105313. https://doi.org/10.1002/advs.202105313.

[24] S. Murmu, S. Paul, A. Santra, M. Robert, U. K. Ghorai, Graphene wrapped nickel phthalocyanine nanohybrid: Efficient electrocatalyst for nitrogen reduction reaction, Catal. Today, 423 (2023), 113938. https://doi.org/10.1016/j.cattod.2022.10.020.

[25] G. W. Watt, J. D. Chrisp, Spectrophotometric Method for Determination of Hydrazine, Anal. Chem., 24 (1952), 12, 2006–2008. https://doi.org/10.1021/ac60072a044.

[26] G. F. Chen, Y. Yuan, H. Jiang, S.Y. Ren, L.X. Ding, L. Ma, T. Wu, J. Lu, H. Wang, Electrochemical reduction of nitrate to ammonia via direct eight-electron transfer using a copper–molecular solid catalyst, Nat Energy, 5 (2020), 605–613. https://doi.org/10.1038/s41560-020-0654-1.

[27] A. Adalder, S. Paul, N. Barman, A. Bera, S. Sarkar, N. Mukherjee, R. Thapa, U. K. Ghorai, Controlling the Metal–Ligand Coordination Environment of Manganese Phthalocyanine in 1D–2D Heterostructure for Enhancing Nitrate Reduction to Ammonia, ACS Catal., 13 (2023), 13516–13527. https://doi.org/10.1021/acscatal.3c02747.

[28] S. Sarkar, A. Adalder, S. Paul, S. Kapse, R. Thapa, U. K. Ghorai, Iron phthalocyanine hollow architecture enabled ammonia production via nitrate reduction to achieve 100 % Faradaic efficiency, Appl. Catal. B: Environ., 343 (2024), 123580. https://doi.org/10.1016/j.apcatb.2023.123580.

[29] N. Mukherjee, A. Adalder, N. Barman, R. Thapa, R. Urkude, B. Ghosh, U. K. Ghorai, $Fe(TCNQ)_2$ nanorod arrays: an efficient electrocatalyst for electrochemical ammonia synthesis via the nitrate reduction reaction, J. Mater. Chem. A, 12 (2024), 3352-3361.

https://doi.org/10.1039/D3TA05300H.

[30] G. Zhu, X. Xie, X. Li, Y. Liu, X. Shen, K. Xu, S. Chen, Nanocomposites Based on $CoSe_2$-Decorated $FeSe_2$ Nanoparticles Supported on Reduced Graphene Oxide as High-Performance Electrocatalysts toward Oxygen Evolution Reaction, ACS Appl. Mater. Interfaces, 10 (2018), 19258–19270. https://doi.org/10.1021/acsami.8b04024.